# Using Molecular Dynamics to Assess Mechanical Properties of PAN-Based Carbon Fibers Comprising Imperfect Crystals with Amorphous Structures

A. Ito, S. Okamoto

**Abstract**—We constructed an atomic structure model for a PAN-based carbon fiber containing amorphous structures using molecular dynamics methods. It was found that basic physical properties such as crystallinity, Young's modulus, and thermal conductivity of our model were nearly identical to those of real carbon fibers. We then obtained the tensile strength of a carbon fiber, which has no macro defects. We finally determined that the limitation of the tensile strength was 19 GPa.

**Keywords**—Amorphous, carbon fiber, molecular dynamics, tensile strength.

### I. INTRODUCTION

ARBON fibers have reduced the weight of structural subassemblies. As a result, they are being employed as advanced industrial materials in airplanes and sporting gear. However, the strength of real carbon fibers is less than 5% of the theoretical strength (110-130 GPa) of graphene [1], [2], which is the basic structure of carbon fibers. This decrease in strength appears to be caused by various types of defects, including vacancies [3], hetero atoms [4], grain boundaries [5], disarray of crystalline orientation [6], and macro defects. Our goal is to clarify the relation between atomic-scale structures and mechanical properties of carbon fibers using molecular dynamics (MD) simulations. Carbon fibers are mainly classified into two types: polyacrylonitrile (PAN)- and pitch-based carbon fibers. PAN-based carbon fibers, which are currently used commonly, have a complicated structure that contains both crystalline and amorphous regions [7].

MD simulations of carbon fiber orientation parameters and grain boundaries are yet to be determined. Additionally, MD simulations of the carbon fibers amorphous structures have yet to be reported. We constructed a PAN-based carbon fiber model and estimated the limitation of the carbon fiber tensile strength that contains no macro defects.

## II. METHODS

The MD calculations in this study were conducted using the Verlet method to calculate the time integral of the equations of motion of atoms. The velocities of all atoms were simultaneously adjusted using the velocity scaling method [8] to control the temperature of the object model to a preset temperature, TSET. The mass of carbon atoms, mC, is  $1.9927 \times 10-26 \, \mathrm{kg}$ . The time step was set at  $0.2 \, \mathrm{fs}$ .

## A. Construction of a Carbon Fiber Model

The second generation reactive empirical bond order (second REBO) potential [9] was used for the covalent C-C bonds. The Lennard-Jones (LJ) potential was used for the van der Waals force between graphene sheets. The use of the second REBO and LJ potentials was switched, according to the interatomic distances and bond orders [10].

The procedure for constructing a carbon fiber model consists of three steps: formation of grain boundaries, generation of vacancies, and promotion of amorphous structures growth by annealing. For the formulation of grain boundaries, 32 graphite crystallites containing 131,880 atoms, which have orientation angles of  $\pm 0^{\circ}$ ,  $\pm 10^{\circ}$ ,  $\pm 20^{\circ}$ , or  $\pm 30^{\circ}$ , against the fiber axis, were used to create a multi-crystalline graphite structure. Each crystallite consists of approximately 4,000 carbon atoms with dimensions equal to that of the real carbon fiber crystallite [11] as shown in Fig. 1.

Crystallites with an individual orientation angle were arranged in  $4\times2\times4$  matrix such that the global orientation degree used as the orientation parameter was around 80% as shown in Fig. 2.

Next, grain boundaries were formed between the crystallites under the periodic boundary conditions in all three directions in the isothermal-isobaric (NPT) ensemble. In the NPT ensemble, number of atoms (N), pressure (P), and temperature (T), are constant. The pressure was controlled using the Parrinello-Rahman method [12]. The preset temperature and pressure were 300K and 1atm, respectively. After the grain boundaries were formed, vacancies were generated by randomly removing carbon atoms from the model until the porosity reached 9.9%. This brought the total number of atoms to 118,774.

We used only the second REBO potential, and not the LJ potential, in order to easily develop amorphous structures in the model during the process of annealing. The periodic boundary conditions were imposed in all three directions. MD

A. Ito is with the Composite Materials Research Laboratories, Toray Industries, Inc., Masaki-cho 791-3196, Japan (phone: +81-89-960-3842; fax: +81-89-960-3834; e-mail: Akihiko Ito@ nts.toray.co.jp).

S. Okamoto is with the Graduate School of Science and Engineering, Ehime University, Matsuyama 790-8577, Japan (e-mail: okamoto.shingo.mh@ehime-u.ac.jp).

This work was supported by JKA (25-100) and its promotion funds from KEIRIN RACE.

annealing simulations were performed in the canonical (NVT) ensemble. In the NVT ensemble, number of atoms (N), volume (V), and temperature (T), are constant. The annealing procedure is described as follows: First, the analysis model was relaxed at the preset temperature of 1,000–2,000K for a preset period of 3.6ps. The analysis model was then cooled down to 300K in steps of 0.5K and then relaxed at 300K for a preset time.

Finally, the model was relaxed with the second REBO and LJ potentials under the periodic boundary conditions in the Y and Z directions at 300K for 7000 MD steps.

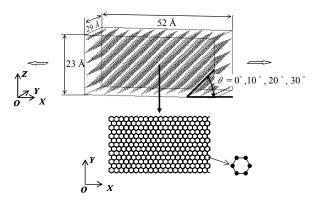


Fig. 1 Configuration of a single-crystalline graphite consisting of about 4,000 atoms with an individual orientation angle

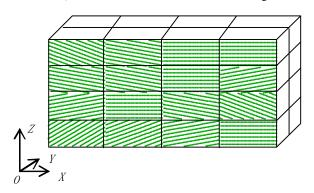


Fig. 2 Configuration of the 32 crystallites of graphite consisting of 131,880 atoms before the formulation of grain boundaries

## B. Validation of the Carbon Fiber Model

We tested the carbon fiber model to determine the basic physical properties of the carbon fibers. The orientation parameter was calculated by the  $\beta$ -scan method [13], based on the X-ray diffraction (XRD) theory [14]. The intensity of XRD,  $I_m$ , is given by (1) and (2):

$$I_{m} = f(s)^{2} \left\{ N + \sum_{j \neq k} \cos 2\pi (\boldsymbol{b} \cdot \boldsymbol{r}_{jk}) \right\}$$

$$s = \sin \theta / \lambda$$
(1)

where f(s) denotes the atomic scattering factor of a carbon atom [15], and N is the number of atoms in a fundamental cell. The vector  $\mathbf{b}$  is a reciprocal space vector with a length  $|\mathbf{b}|$  of 2s

and direction  $(\mathbf{k}_{d} - \mathbf{k}_{i})$ , where  $\mathbf{k}_{i}$  and  $\mathbf{k}_{d}$  are the wavenumber vectors of the incident and diffracted waves, respectively. The vector  $\mathbf{r}_{jk}$  is a vector from atoms j to k, while  $\lambda$  is the wavelength of the X-ray.  $2\theta$  is the diffraction angle.

The measurement principles of the  $\beta$ -scan method are shown in Fig. 3.  $2\theta$  was set to the diffraction angle of the (002) plane, i.e.  $25.5^{\circ}$ , to determine the orientation of the (002) plane in a graphite crystallite to the *X*-axis. The wavelength of the CuK $\alpha$  X-ray was set to 1.54 Å. The  $\beta$ -axis was parallel to the *Y*-axis. The X-ray enters at an angle of (90- $\theta$ ) $^{\circ}$  (0 $\leq \theta \leq 90^{\circ}$ ) with  $\boldsymbol{b}$  and is detected at the same angle as an incident wave. The theoretical diffraction spectra are obtained by calculating  $I_m$  using (1) and rotating  $\boldsymbol{b}$  about the  $\beta$ -axis.

In the present study, the diffraction spectra were calculated every 1.0°. The calculated spectrum was then approximated with a normal distribution function (NDF) using the least squares method.

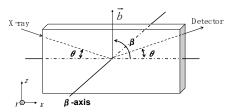


Fig. 3 Measurement principles of the  $\beta$ -scan method using X-ray diffraction

The full width,  $\Delta\xi$  ( 0°–180°) at a half-maximum (FWHM) of the normal distribution function can be determined using the approximated NDF. In the present study, the orientation parameter  $\Pi$  is defined as

$$\Pi = 1 - \frac{\Delta \xi}{180} \tag{3}$$

The crystallinity, the crystallite sizes (Lc) in the c axis, and the interlayer spacing between graphene sheets were obtained using powder XRD simulations. The average intensity of XRD  $< I_m >$  was calculated using [14];

$$\langle I_m \rangle = f(s)^2 \left\{ N + \sum_{j \neq k} \frac{\sin 2\pi |\boldsymbol{b}| \boldsymbol{r}_{jk}}{2\pi |\boldsymbol{b}| \boldsymbol{r}_{jk}} \right\}$$
(4)

The crystallinity was calculated from the theoretical XRD spectrum using

where (A), (B), (C), and (D) denote the total intensity of XRD from the graphite (002) plane of perfect graphite, the total intensity from the analysis model, the mass density of perfect graphite, and mass density of the analysis model, respectively.

Lc was calculated from the FWHM of the (002) plane using Scherrer's equation [16]

$$L_{C} = \frac{K\lambda}{\beta_{0} \cos \theta_{B}}$$
 (6) 
$$g(t) = A_{o} \exp\left(\frac{-t}{\tau_{o}}\right) + A_{a} \exp\left(\frac{-t}{\tau_{a}}\right)$$
 (11)

where

$$\beta_0 = \left(\beta_E^2 - \beta_I^2\right)^{1/2} \tag{7}$$

and K is a coefficient.  $\lambda$ ,  $\beta_E$ , and  $\theta_B$  denote the X-ray wavelength, the FWHM of the peak, and Bragg angle, respectively. The values of K and  $\beta_I$  are 1.0 and  $1.05 \times 10^{-2}$  rad, respectively.

The interlayer spacing,  $d_{002}$ , was obtained using the Bragg equation:

$$2d_{002}\sin\theta_{002} = \lambda \tag{8}$$

where  $\theta_{002}$  denotes the position of the peak of (002) plane.

There are many possible theoretical approaches for determining the thermal conductivity from molecular simulations. One approach is the use of non-equilibrium MD (NEMD) simulations [17], [18]. Here, a body is subjected to a unidirectional temperature gradient, and the thermal conductivity is obtained from the transfer rate of the thermal energy through a material of certain thickness using Fourier's law. Another approach is the use of equilibrium MD (EMD) simulations [19], [20], which use the Green-Kubo relations. In our present work, EMD simulations were used to estimate the thermal conductivities quantitatively because the thermal conductivities obtained by NEMD are usually an order of magnitude smaller than experimentally obtained results. The Green-Kubo relation is

$$\lambda = \frac{1}{k_R T^2 V} \int_0^\infty dt \langle \boldsymbol{J}_X(0) \cdot \boldsymbol{J}_X(t) \rangle \tag{9}$$

where  $\lambda$ ,  $k_B$ , T, V, and  $J_X(t)$  denote the thermal conductivity, Boltzmann constant, temperature, volume of the fundamental cell, and heat current vector in the X direction, respectively.

The EMD simulations were performed as follows: First, the models were relaxed at 300 K for 50,000 MD steps in the NVT ensemble using the velocity scaling method. Then, the heat current vectors were calculated for 140,000 MD steps in the microcanonical (NVE) ensemble, i.e. constant number of atoms, volume, and energy.

Next, the auto-correlation function, COR (t), was calculated using

$$COR(m\Delta t) = \frac{1}{N-m} \sum_{n=0}^{N-m} \boldsymbol{J}_X ((n+m)\Delta t) \boldsymbol{J}_X (n\Delta t)$$
 (10)

where N and  $\Delta t$  denotes the total number of MD steps and time step, respectively. The auto-correlation function results corresponding to the first 3 ps were fitted using the least-squares method to the double exponential function, g(t) according to Grujicic's method [19]

where the subscripts o and a are used to denote the optical and acoustic phonon modes, respectively. Finally, the thermal conductivity was obtained by integrating g(t).

C. Estimation of the Limitation of the Tensile Strength

We performed MD simulations on the tensile loading of the model in order to estimate the limitation of the tensile strength. In the MD simulations, the Tersoff potential [21] was used for the covalent C-C bonds in order to reduce the computational time. The LJ potential was used to determine the interlayer interactions between graphene sheets. Periodic boundary conditions were imposed in the Y and Z directions. The analysis model consisted of two parts: the active and boundary zones. In the active zone, the atoms move according to their interactions with neighboring atoms. In contrast, in the boundary zone, enclosed by the boxes in Fig. 4, the atoms are constrained. The thickness l of the boundary zone is  $4.5a\sqrt{3}/4$ where a is the length of a graphene C=C bond. The pressure  $P_{IJ}$  and stress  $\sigma_{IJ}$  for the X, Y, and Z directions are obtained by calculating the kinetic energies of, and the interatomic force on, the atoms in the fundamental cell and can be written as

$$P_{IJ} = \frac{1}{V} \left( \sum_{i \in V} m \overline{v_I^i v_J^i} + \sum_{i \in V} I^i F_J^i \right) \qquad (I = x, y, z; J = x, y, z) \quad (12)$$

$$\sigma_{IJ} = \frac{1}{V} \left( \sum_{i \in V} m \overline{v_I^i v_J^i} + \sum_{i \in V} \overline{I^i F_J^i} \right) - P \quad (I = x, y, z; J = x, y, z)$$
 (13)

where V denotes the volume, m is the mass of the carbon atoms,  $v^i_I$  is the velocity of atom i in the I direction,  $F^i_J$  is the interatomic force acting on atom i in the J direction, and P represents the external pressure.

The pressure was adjusted by controlling the volume of the fundamental cell using (14) such that the components orthogonal to the tensile axis, i.e. the Y and Z-components for the analysis model under tension in the X direction, of the output stress tensor can be zero for each strain [22].

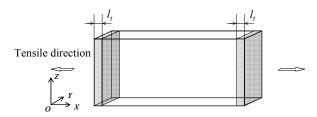


Fig. 4 Multicrystalline graphite configuration for tensile loading

$$L_{I}(1 + \alpha_{I}(P_{I} - P_{SET})) \rightarrow L_{I}$$
(14)

where  $L_I$  represents the length of the fundamental cell in the I

direction.  $P_{\text{SET}}$  is the preset pressure, and  $\alpha_I$  is an appropriate constant. In this work,  $P_{\text{SET}}$  was set to 1atm, while  $\alpha_I$  was set to 0.03

The atomic stress acting on each atom was calculated to obtain the stress-strain curves. The atomic stress  $\sigma^i_J$  for each direction of J is obtained by calculating the kinetic energies of, the interatomic force acting on, and the volume occupied by atom i as

$$\sigma^{i}_{IJ} = \frac{1}{\Omega^{i}} \left( m \overline{v^{i}_{I} v^{i}_{J}} + \overline{I^{i} F^{i}_{J}} \right) (I = x, y, z; J = x, y, z), \quad (15)$$

where  $\Omega^i$  represents the volume occupied by atom i, and is referred to as the atomic volume.  $\Omega^i$  is calculated by averaging the volume over all of the atoms in the initial structure of each system. The interatomic force acting on atom i by its neighboring atoms in the J direction is represented as  $F^i_J$ .

The tensile loading methods were as follows: First, the atoms of the analysis model were relaxed to stabilize the stresses for 7,000 MD simulation steps. The atoms in the active zone were relaxed in all directions. The atoms in the boundary zone were relaxed only in the Y and Z directions. After the atoms were relaxed, constant displacements were applied to the atoms in the boundary zones during each MD step to simulate uniaxial tensile loading in the X direction. The atoms inside the boundary zones were contrained in the X and Y directions. The atoms in the active zone of the analysis model were relaxed for all directions, while those in the boundary zones were only relaxed in the Z direction. The volume of the analysis model was then adjusted every 50 MD steps using (14) such that the Y and Z components of the output stress tensor were zero for each strain. The strain increment  $\Delta \varepsilon$  was set to 5.7×10<sup>-7</sup> per step. The Young's modulus was obtained from the slopes of the straight lines in the range, where the relation between the stress and strain is linear. The tensile strength was given by the peak of the nominal stress-strain curves.

# III. RESULTS AND DISCUSSION

# A. Construction of a Carbon Fiber Model

For the annealing case at 2,000 K, the structure changes before and after annealing as shown in Fig. 5. It was found that the sp³ carbons, shown by a red circle in Fig. 5, increased in number after annealing. Overall, amorphous structures, which do not resemble graphite, increased. In addition, a cross-sectional image of the model in the longitudinal direction is shown in Fig. 6. No boundaries seem to be present between the amorphous and crystalline structures. The layers inside the crystal regions orientate to the fiber axis. Thus, the structure of the carbon fiber model obtained by the annealing is nearly identical to the TEM image shown in Fig. 6.

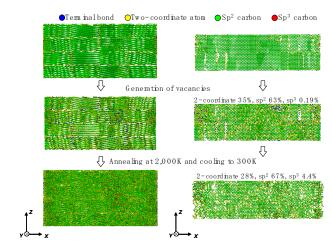


Fig. 5 PAN-based carbon fiber model containing amorphous structures

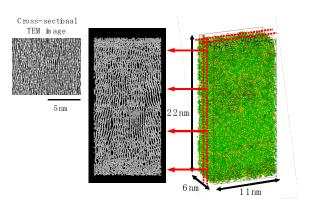


Fig. 6 Cross-section of PAN-based carbon fiber model compared to the high-resolution TEM image of the T800G fiber

TABLE I
BASIC PHYSICAL PROPERTIES OF CARBON FIBERS

BASIC I ITTSICAL I ROLLKTIES OF CARBON I IBERS								
Material	d Å	f %	Lc Å	$d_{002}  m \AA$	П %	λ W/mK	E GPa	<i>G</i> GPa
MD								
PAN-CF	1.80 <sup>a</sup>	47	20	3.47	81	32.5	287ª	$26.9^{a}$
Exp.								
T800G <sup>b</sup>	1.80 <sup>b</sup>	51 <sup>b</sup>	$20^{\mathrm{b}}$	3.48°	82 °	_	255 <sup>b</sup>	$27.1^{b}$
T800H	1.81 <sup>d</sup>	_	_	_	83 <sup>e</sup>	$35.1^{d}$	294	25 e
T1000G <sup>d</sup>	1.80	_	_	_	_	32.0	294	21.6

d: mass density, f: crystallinity, Lc: crystal size,  $d_{002}$ : interlayer spacing,  $\Pi$ : orientation parameter,  $\lambda$ : thermal conductivity, E: Young's modulus, G: shear modulus

a: corresponding value as the porosity the model is equal to that of the  $T800G\ fiber$ 

b: [23], c: [24], d: [25], e: [26]

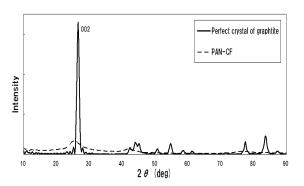


Fig. 7 Powder XRD spectra of a graphite crystal and PAN-CF model

## B. Validation of the Carbon Fiber Model

The basic physical properties of the (PAN-CF) model are shown in Table I and are compared with the experimental results of the actual PAN-based carbon fibers [23]-[26]. The data of the moderate-modulus carbon fibers, whose orientation parameters are nearly identical to the PAN-CF model, were cited.

For all the cases, the basic physical properties of the PAN-CF model agree well with the experimental results. The calculated powder XRD spectra of the graphite crystal and -CF models are shown in Fig. 7. The PAN-CF model peak became broad due to the development of amorphous structures.

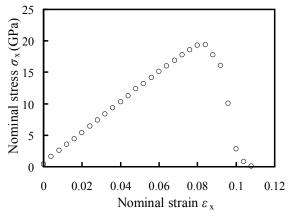


Fig. 8 Stress-strain plots of the PAN-CF model

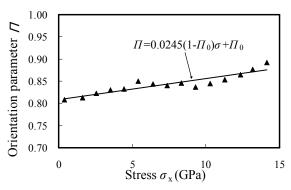


Fig. 9 Relation between the orientation parameter and stress

## C. Estimation of the Limitation of the Tensile Strength

The stress-strain plots of the PAN-CF are shown in Fig. 8. The PAN-CF tensile strength is 19 GPa. The calculated tensile strength was higher when compared with the actual carbon fibers (up to 7 GPa) because of the absence of macro defects.

The change of the orientation parameter  $\Pi$  under tensile loading is shown in Fig. 9.  $\Pi$  increased with increasing stress  $\sigma_X$ . The relation between  $\Pi$  and  $\sigma_X$  was estimated using a straight line by the least squares method. The relation equation is

$$\Pi = 0.025(1 - \Pi_0)\sigma + \Pi_0 \tag{16}$$

where  $\Pi_0$  denotes the initial orientation parameter. Equation (16) agrees with the empirical equation determined by Shioya et al. [27]

$$\Pi = 0.029(1 - \Pi_0)\sigma + \Pi_0 \tag{17}$$

Thus, it was found that the change in the orientation parameter under tensile loading agrees with the experimental results

### IV. CONCLUSION

We successfully constructed the atomic structure using a PAN-based carbon fiber model whose basic physical properties, such as crystallinity, Young's modulus, and thermal conductivity were nearly identical to those of the actual materials. This was accomplished by annealing the multi-crystalline graphite model consisting of the crystallites with the individual orientation angle. In addition, we performed tensile loading MD simulations on the PAN-based carbon fibers model and clarified the limitation of its tensile strength. Future work could involve the creation of high-performance carbon fibers by investigation of the effects of structural parameters, such as the orientation parameter and crystal size based on the PAN-based carbon fibers model and by clarifying the ideal structure of the carbon fiber.

## REFERENCES

- C. Lee, X. Wei, J. W. Kysar, and J. Hone, "Measurement of the elastic properties and intrinsic strength of monolayer graphene," *Science*, vol. 321, pp. 385-388, Jul. 2008.
- [2] F. Liu, P. Ming, and J. Li, "Ab initio calculation of ideal strength and phonon instability of graphene under tension," *Phys. Rev. B*, vol. 76, pp. 064120, Aug. 2007.
- [3] A. Ito and S. Okamoto, "Molecular Dynamics Analysis on Effects of Vacancies upon Mechanical Properties of Graphene and Graphite," *Engineering Letters*, vol. 20, pp. 271-278, Aug. 2012.
- [4] S. Okamoto and A. Ito, "Effects of Nitrogen Atoms on Mechanical Properties of Graphene by Molecular Dynamics Simulations," *Engineering Letters*, vol. 20, pp. 169-175, May 2012.
- [5] R. Grantab, V. B. Shenoy, R. S. Ruoff, "Anomalous strength characteristics of tilt grain boundaries in graphene," *Science*, vol. 330, pp. 946-948, Nov. 2010.
- [6] A. Ito and S. Okamoto, "Effect of orientation parameters of multicrystalline graphites on mechanical properties by molecular dynamics simulations," in *Proc. 4th International Conference on Computational Methods*, Gold Coast, CD-ROM, Nov. 2012.
- [7] O. Paris, D. Loidl, H. Peterlik, "Texture of PAN- and pitch-based carbon fibers," *Carbon*, vol. 40, pp. 551-555, Apr. 2002.

- [8] L. V. Woodcock, "Isothermal molecular dynamics calculations for liquid salts," *Chem. Phys. Lett.*, vol. 10, pp. 257-261, Aug. 1971.
- [9] D. W. Brenner, O. A. Shenderova, J. A. Harrison, S. J. Stuart, B. Ni, and S. H. Sinnott, "A second-generation reactive empirical bond order (REBO) potential energy expression for hydrocarbons," *J. Phys. Condens. Mat.*, vol. 14, pp.783-802, Jan. 2002.
- [10] S. J. Stuart, A. B. Tutein, and J. A. Harrison, "A reactive potential for hydrocarbons with intermolecular interactions," *J. Chem. Phys.*, vol. 112, no. 14, pp. 6472-6486, Jan. 2000.
- [11] D. J. Johnson, "Handbook of polymer-fibre composites," Longman Publishing Group, 1994, pp. 24-29.
- [12] M. Parrinello and A. Rahman," Polymorphic transitions in single crystals: A new molecular dynamics method," *Journal of Applied Physics*, vol. 52, pp. 7182-7190, Aug. 1981.
- [13] S. Okamoto and A. Ito, "Molecular dynamics simulations on multicrystalline graphite containing grain boundaries," in *Proc. Society* for the Advancement of Material and Process Engineering, Baltimore, CD-ROM, May. 2012.
- [14] M. Kakudo and N. Kasai, "X-ray diffraction by macromolecules," Elsevier B.V., 2005.
- [15] E. Prince, "International Tables for Crystallography (Volume C)," Wiley/International union for crystallography, 2004.
- [16] N. S. Saenko, "The X-ray diffraction study of three-dimensional disordered network of nanographites: experiment and theory," *Physics Procedia*, vol. 23, pp. 102-105, 2012.
- [17] C. W. Padgett and D. W. Brenner, "Influence of chemisorption on the thermal conductivity of single-wall carbon nanotubes," *Nano Lett.*, vol. 4, pp. 1051-1053, May 2004.
- [18] T. Y. Ng, J. J. Yeo, and Z. S. Liu, "A molecular dynamics study of the thermal conductivity of graphene nanoribbons containing dispersed Stone-Thrower-Wales defects," *Carbon*, vol. 50, pp. 4887-4893, Jun. 2012
- [19] M. Grujicic, G. Cao, and B. Gersten, "Atomic-scale computations of the lattice contribution to thermal conductivity of single-walled carbon nanotubes," *Materials Science and Engineering B*, vol. 107, pp. 204-216, Mar. 2004.
- [20] H. Zhang, G. Lee, and K. Cho, "Thermal transport in graphene and effects of vacancy defects," *Phys. Rev. B*, vol. 84, pp. 115460, Sep. 2011
- [21] J. Tersoff, "Modeling solid-state chemistry: interatomic potentials for multicomponent systems," *Phys. Rev. B*, vol. 39, no. 8, pp.5566-5568, Mar., 1989.
- [22] Izumi, S. and Kotake, S. "Molecular Dynamics Study of Solid Deformation," *Transaction of the Japan Society of Mechanical Engineers (in Japanese) A*, vol. 59, pp. 263-267, Jan. 1993.
- [23] F. Tanaka, T. Okabe, H. Okuda, M. Ise, I. A. Kinloch, T. Mori, R. J. Young, "The Effect of Nanostructure upon the Deformation Micromechanics of Carbon Fibres," *Carbon*, vol.52, pp. 372-378, Feb. 2013
- [24] F. Tanaka, T. Okabe, H. Okuda, I. A. Kinloch, R. J. Young, "The Effect of Nanostructure upon the Compressive Strength of Carbon Fibres," *Journal of Materials Science*, vol. 48, pp. 2104-2110, Mar. 2013.
- [25] A. Shindo, "Polyacrylonitrile (PAN)-based Carbon Fibers' Comprehensive Composite Materials, vol. 1, 2000, pp. 1-33.
- [26] K. Honjo, "Fracture toughness of PAN-based carbon fibers estimated from strength-mirror size relation", *Carbon*, vol. 41, pp. 979-984, 2003.
- [27] M. Shioya, E. Hayakawa, A. Takaku, "Non-hookean stress-strain response and changes in crystallite orientation of carbon fibers", J. Mat. Sci., vol. 31, pp. 4521-4532, Jan. 1996.